Geological Society of America
Special Paper 356
2002

Complex tsunami waves suggested by the Cretaceous-Tertiary boundary deposit at the Moncada section, western Cuba

R. Tada
Y. Nakano
Department of Earth and Planetary Science, Graduate School of Science, University of Tokyo, 7-3-1 Hongo, Tokyo 113-0033, Japan
M.A. Iturralde-Vinent
Museo Nacional de Historia Natural, Obispo no. 61, Plaza de Armas, La Habana 10 100, Cuba
S. Yamamoto
T. Kamata
E. Tajika
Department of Earth and Planetary Science, Graduate School of Science, University of Tokyo, 7-3-1 Hongo, Tokyo 113-0033, Japan
K. Toyoda
Graduate School of Environmental Earth Science, Hokkaido University, N17 W8, Sapporo 060-0810, Japan
S. Kiyokawa
Department of Earth and Planetary Sciences, Faculty of Sciences, Kyushu University 33 Hakozaki, Fukuoka 812-8581, Japan
D. Garcia Delgado
Instituto de Geologia y Paleontologia, Via Blanca y Linea del Ferrocarril San Miguel del Padron, La Habana 11 000, Cuba
T. Oji
K. Goto
H. Takayama
NHK Japan Broadcasting Corporation, Nagoya Office 1-13-3 Higashisakura, Higashiku, Nagoya 461-8725, Japan
R. Rojas
Museo Nacional de Historia Natural, Obispo no. 61, Plaza de Armas, La Habana 10 100, Cuba
T. Matsui
Department of Complexity Science and Engineering, Graduate School of Frontier Science, University of Tokyo, 7-3-1 Hongo, Bunkyo-ku, Tokyo 113-0031, Japan

ABSTRACT

The Moncada Formation in western Cuba is an ~2-m-thick weakly metamorphosed complex characterized by repetition of calcareous sandstone units that show overall upward fining and thinning. The Moncada Formation contains abundant shocked quartz, altered vesicular impact-melt fragments, and altered and deformed greenish grains of possible impact glass origin. In addition, a high iridium (~0.8 ppb)

Tada, R., Nakano, Y., Iturralde-Vinent, M.A., Yamamoto, S., Kamata, T., Tajika, E., Toyoda, K., Kiyokawa, S., Garcia Delgado, D., Oji, T., Goto, K., Takayama, H., Rojas, R., and Matsui, T., 2002, Complex tsunami waves suggested by the Cretaceous-Tertiary boundary deposit at the Moncada section, western Cuba, *in* Koeberl, C., and MacLeod, K.G., eds., Catastrophic Events and Mass Extinctions: Impacts and Beyond: Boulder, Colorado, Geological Society of America Special Paper 356, p. 109–123.

peak is identified at the top of the formation. Together with the biostratigraphically estimated age, between late Maastrichtian and early Paleocene, this evidence supports a Cretaceous-Tertiary (K-T) boundary origin for the deposit. The Moncada Formation has ripple cross-laminations at several horizons that indicate north-south–trending paleocurrent directions with reversals. Changes in detrital provenance corresponding to paleocurrent reversals are also recognized. These characteristics are similar to K-T boundary sandstone complexes reported from the Gulf of Mexico region, and strongly support a K-T boundary tsunami origin for the Moncada Formation. The pattern of paleocurrent reversals in the Moncada Formation suggests that tsunami waves were not simple alternations of a single beat, but rather alternations of double beats following the first wave that came from the south. In addition, the maximum grain-size variation within each unit suggests the presence of higher frequency waves superimposed on the lower frequency waves. Thus, our results suggest that K-T impact tsunami waves had a complex rhythm that was caused either by reflections and diffractions of waves or by multiple tsunami waves created by multiple gravity-flows triggered by seismic shocks of the impact.

INTRODUCTION

Since the discovery of the Cretaceous-Tertiary (K-T) boundary impact crater at Chicxulub, Yucatan (Hildebrand et al., 1991), the focus of K-T boundary research has shifted toward exploring the environmental consequences of the K-T impact (e.g., Ryder et al., 1996; D'Hondt et al., 1994). A giant tsunami is one of the probable consequences, and possible K-T boundary tsunami deposits have been reported at many localities in the marginal part of the Gulf of Mexico (e.g., Bourgeois et al., 1988; Smit et al., 1992, 1996; Smit, 1999). However, their origin is still controversial and an impact-induced megaturbidite origin has also been advocated (Bohor, 1996).

The Late Cretaceous to early Tertiary sedimentary sequence is widely distributed throughout the Cuban fold belt, and extraordinarily thick (to 700 m), coarse-grained event deposits, usually dated as upper Maastrichtian, have been known for some time in the sections of central and western Cuba (Pszczolkowski, 1986; Iturralde-Vinent, 1992). Although their megaturbidite origin, and a possible relation with the K-T bolide impact, was advocated by Pszczolkowski (1986), not enough evidence was presented to demonstrate a megaturbidite origin, and the relation with the K-T boundary impact remained controversial, because no conclusive evidence was presented to support their K-T boundary age (e.g., Iturralde-Vinent, 1992). Takayama et al. (2000) reported latest Maastrichtian nannofossils, *Micula prinsii*, from a mudstone intraclast in the deposit near Havana, Cuba (the Peñalver Formation). Together with their discovery of shocked quartz from the same deposit, these authors concluded that the deposit was formed in association with the K-T bolide impact. They also argued that the deposit consists of a lower gravity-flow unit and an upper homogenite (a deep-sea tsunami deposit) unit, and proposed the occurrence of deep-sea tsunamis at K-T boundary sites in western Cuba.

Although most of the K-T boundary deposits in western and central Cuba are characterized by thick, coarse-grained deposits (Takayama et al., 2000, Iturralde-Vinent et al., 2000, Kiyokawa et al., 2000), a relatively thin (~2 m) calcareous sandstone of probable K-T boundary age is present in the Los Organos belt of the Guaniguanico terrane in western Cuba (Iturralde-Vinent, 1995). Such a thin (compared to other K-T boundary sites in western Cuba) deposit needs to be explained, and the answer may give a clue to solving the origin and extent of tsunami waves at the K-T boundary.

In this chapter we describe the occurrence of this 2-m-thick deposit, present evidence to support its association with the K-T boundary impact, and discuss the origin of the deposit and its implication for the nature of tsunamis. The observation suggests a complex behavior of tsunami waves immediately following the impact in the eastern margin of the Yucatan platform.

GEOLOGICAL SETTING OF WESTERN CUBA

The present Cuban fold belt contains five geotectonic units; the autochthonous Bahamian platform, the allochthonous southwestern Cuba terranes (the Guaniguanico, Escambray, and Pinos terranes), the northern ophiolite and Placetas belts, the Cretaceous volcanic arc, and neoautochthonous postorogenic sedimentary rocks of latest Eocene to recent age (Iturralde-Vinent, 1994, 1995, 1998). The Guaniguanico terrane is located in Pinar del Rio Province of western Cuba, where it occurs as a stack of north- to northwest-thrusted sheets that were emplaced onto the Gulf of Mexico autochthon (Iturralde-Vinent, 1994), probably as a result of collision of the extinct Cretaceous volcanic arc caused by the opening of the rift basins in the western part of the Yucatan basin during the late Paleocene to middle Eocene (Rosencrantz, 1990). The Guaniguanico terrane is exposed on the north side of the Pinar fault; the tectonically upper horizons are exposed to the north (Figure. 1). North and

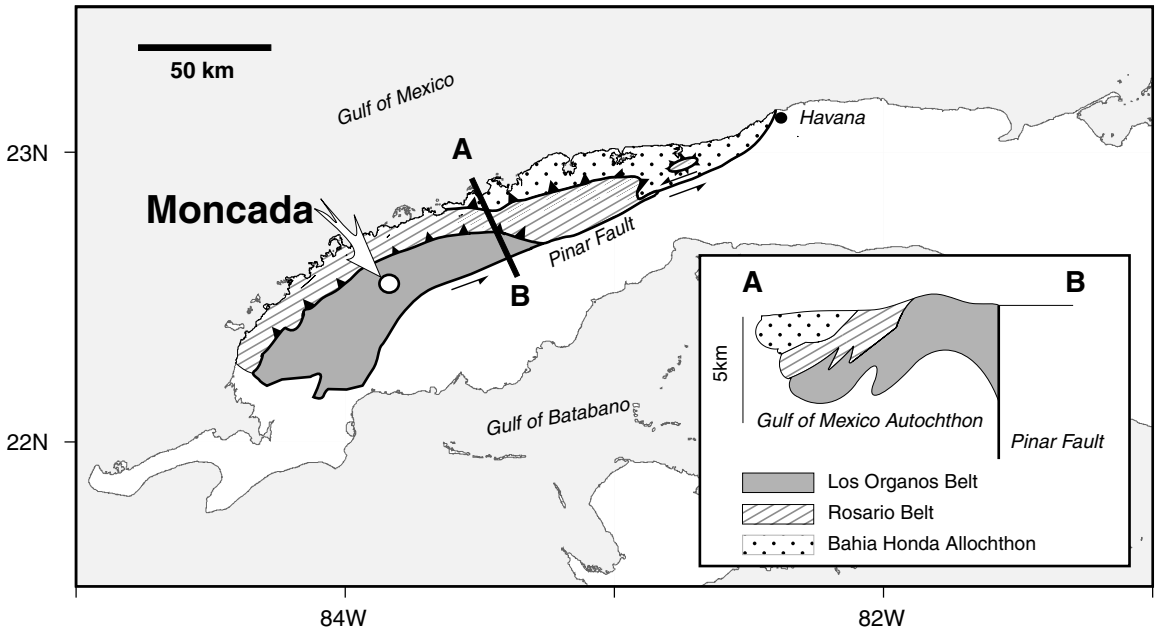

Figure 1. Geologic map of western Cuba showing locality of Moncada section (study site).

east portions of the terrane are tectonically covered by the Bahia Honda allochthon, which is composed of ophiolites, Cretaceous volcaniclastics, and latest Cretaceous to Eocene sedimentary rocks (Iturralde-Vinent, 1994, 1998). The deformation and emplacement of all thrust sheets took place between the late Paleocene and middle Eocene (Bralower and Iturralde-Vinent, 1997).

The allochthonous nature of the Guaniguanico terrane has been discussed in the Cuban literature, and its original location is estimated as the western margin of the Yucatan platform (Iturralde-Vinent, 1994, 1998). It is also considered that the sedimentary sequences of the Guaniguanico terrane originated as a part of the continental margin of the Yucatan platform (Maya block) and the western Caribbean Sea basin (Iturralde-Vinent, 1994, 1998) (Fig. 2). The Moncada section (the site studied in this chapter) occurs in the Los Organos belt, which consists of the thrust sheet at the tectonically lowest position, and includes sedimentary strata of early Middle Jurassic to middle Eocene age (Fig. 1).

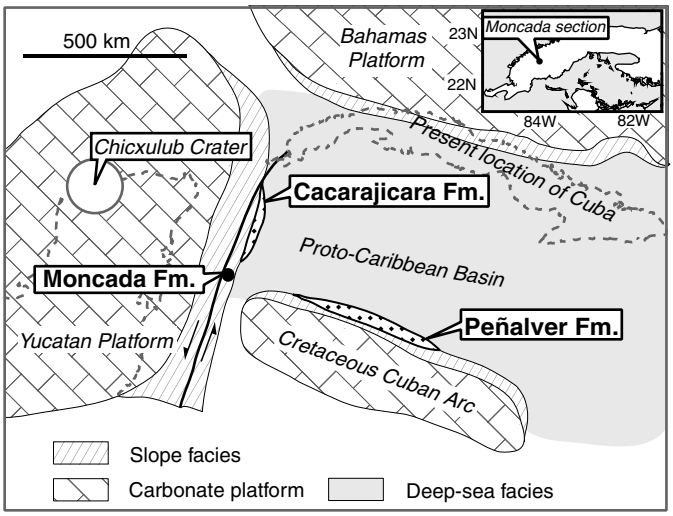

Figure 2. Paleogeotectonic setting of Moncada Formation and other Cretaceous-Tertiary (K-T) boundary deposits in western Cuba at time of K-T impact. Location of Moncada section is also shown in upper right corner of figure. Fm.—Formation.

LOCALITY AND STRATIGRAPHIC SETTING OF THE MONCADA SECTION

The Moncada section is located 18 km to the west of the town of Viñales, along the road to Pons, just at the intersection with the village of Moncada. The section is exposed on both sides of a roadcut immediately to the west of the intersection, where a >40-m-thick sequence of Cretaceous to lower Tertiary strata are exposed. The strata dip gently east; the general strike and dip are N15°-40°E and 8°-12°E, respectively.

Iturralde-Vinent (1995) described a 2-m-thick calcareous sandstone from this locality, which was referred to as the La Güira Member of the Ancón Formation. Bralower and Iturralde-Vinent (1997) paleontologically dated the La Güira Member as early Paleocene (older than NP4). Additional stratigraphic observation in the area suggests that this 2-m-thick calcareous sandstone should be defined as an independent stratigraphic unit, which crops out only in the Moncada section, so it is named the Moncada Formation. The ~2-m-thick Moncada Formation is exposed near the western end of the roadcut. It

disconformably overlies thick-bedded, grayish-black, micritic limestone of the Pons Formation, which yields microfossils of Albian-Cenomanian age. It is conformably overlain by well-bedded, light violet, gray, and greenish-gray micritic slaty limestone of the Ancón Formation, which dates from the late early Paleocene (older than NP4) to the earliest Eocene (P6a) (Bralower and Iturralde-Vinent, 1997). Diaz Otero et al. (2000) reported a mixed microfossil assemblage from the Moncada Formation, the ages ranging from Aptian to late Maastrichtian. Together with the early Paleocene age of the Ancón Formation, this result suggests an age between late Maastrichtian and early Paleocene for the Moncada Formation.

SAMPLES AND METHODS

The entire sequence of the Moncada Formation, as well as the strata immediately above and below it, were sampled almost continuously, using a motor-powered cutter. Sedimentary structures were observed and described on the cut surfaces. Rough estimation of the current directions was conducted for cross-laminated intervals in field based on observation of the differently orientated cut surfaces. In addition, orientated samples were taken for such intervals to estimate current directions based on three-dimensional observations of the samples in the laboratory. Each sample, generally representing 5–10 cm of stratigraphic interval, was polished and sedimentary structures were described. Thin sections were prepared for most of the samples to examine grain composition and the maximum grain size. The maximum grain size of detrital silicate and/or limestone and chert fragments was measured in 1 cm intervals throughout the sequence. Subsamples, each representing 0.5–2-cm-thick intervals, were taken from most of the samples, pulverized, and subjected to X-ray powder diffraction and X-ray fluorescence (XRF) analyses to determine mineral and major element compositions (Tables 1 and 2). Sample preparation and analytical methods for XRD and XRF analyses are the same as those described in Irino and Tada (2000). The reproducibility of XRD measurements is better than $\pm 30\%$ for smectite, illite, and chlorite, $\pm 15\%$ for calcite and plagioclase, and $\pm 10\%$ for quartz. The 2σ relative standard deviation of the XRF measurements is $\pm 0.6\%$–0.8% for SiO_2, TiO_2, Al_2O_3, Fe_2O_3, K_2O, and CaO, and 1.0%–1.2% for MgO, P_2O_5, and loss on ignition, and $\pm 1.4\%$–1.6% for MnO and Na_2O. Identification of smectite and chlorite was carried out for all samples based on glycerol treatment that shifts the 14 Å peak of smectite to ~17.9 Å, and heat treatment at 550°C for 1 h that intensifies the 14.2 Å peak of chlorite and slightly shifts it to 13.8 Å (Moore and Reynolds, 1997). The results suggest that the 14 Å peak is attributed to either smectite or chlorite, whereas the 7 Å peak is attributed to chlorite. Coexistence of chlorite and smectite is identified in some samples. The smectite peak height is corrected for chlorite contribution based on the observation that the 14 Å peak of chlorite is approximately the same in height as its 7 Å peak.

The iridium (Ir) content in selected subsamples was determined by radiochemical neutron activation analysis (RNAA) by irradiation in the JRR-3M reactor of the Japan Atomic Energy Research Institute (JAERI) at a neutron flux of 1.2×10^{14} $cm^{-2}s^{-1}$ for 6 h. Chemical separation was done with Srafion NMRR resin prior to counting on high-resolution Ge detectors at the Central Institute of Isotope Science, Hokkaido University. Recovery of the Ir carrier was 50%–70%, as determined by reactivation. The RNAA procedures were essentially the same as those of Kyte et al. (1992). For the standard, appropriate amounts of diluted solution from Ir standard solution (SIGMA Chemical Co.) were weighed into the quartz tubes immediately after preparation, dried, and then sealed. Our result for SARM7 certified reference material (MINTEK, South African Bureau of Standard) is 73 ± 6 ppb; the reference value of SARM7 from Potts et al. (1992) is 74 ± 12 ppb with 95% confidence intervals. No Ir peaks were observed in blank sample measurement.

MONCADA FORMATION

The Moncada Formation at the Moncada section is 184–191 cm thick, and consists of a calcareous sandstone complex; there are alternations of calcareous claystone and very fine sandstone in the uppermost part of the formation (Fig. 3). The Moncada Formation disconformably overlies grayish-black, bedded micritic limestone of the Pons Formation with a slightly undulating erosional surface (Fig. 4A). The Moncada Formation is conformably overlain by marly limestone of the Ancón Formation with a gradational contact. The sequence is weakly metamorphosed (to pumpellyite facies) and contains some weak shear planes subparallel to the bedding. However, primary fabric and sedimentary structures are still preserved.

Calcareous sandstone complex

The calcareous sandstone complex is characterized by repetition of five sandstone units, with an upward decrease in unit thickness from 93 to 9 cm. The lower two units show a distinct upward fining, whereas the upper three units do not show a clear upward fining (Figure 3). These sandstone units are numbered from 1 to 5 in ascending order. Boundaries between the units are gradational and no erosional contacts are observed. The lower part of each unit is characterized by a thicker, coarser-grained, very thin-bedded, olive-green to light olive, slightly calcareous sandstone compared to the upper part that is characterized by alternations of thinner and finer-grained, parallel to ripple cross-laminated, light gray, calcareous sandstone and grayish-black muddy drapes and/or flasers.

The lower part of unit 1 is composed of faintly stratified and normally graded, very coarse to medium-grained sandstone with occasional intercalations of 1–2-cm-thick granule-rich layers in the basal part. The sandstone is composed of flattened, olive-green grains and angular, whitish, vesicular fragments.

TABLE 1. XRD PEAK INTENSITIES OF CONSTITUENT MINERALS IN BULK SAMPLES

Sample No.	Position (m)	Smectite (cps)	Illite (cps)	Chlorite (cps)	Quartz (cps)	Plagioclase (cps)	Calcite (cps)	Pyroxene (cps)	Rhodochrosite (cps)	Hematite (cps)
Mn32.5	229	0	0	0	175	0	2806	0	58	0
Mn32	227.5	0	6	6	146	0	2582	0	65	10
Mn32-2	227.1	0	0	0	136	0	2710	0	55	0
Mn32-1	225	0	0	0	198	0	2983	0	68	0
Mn31-5	221.6	0	0	0	160	0	2700	0	72	0
Mn31-4	219.8	0	0	0	176	15	2719	0	56	0
Mn31-3	218.4	0	31	0	158	0	2774	0	59	0
Mn31-2	217	0	0	0	150	0	2718	0	74	0
Mn31-1	215.5	0	0	0	138	0	2916	0	68	0
Mn30E-5	214.2	0	0	0	138	0	3056	0	76	0
Mn30E-2	210.9	0	0	0	75	0	2938	0	76	0
Mn30E-1	209.6	0	0	0	58	0	3143	0	68	0
Mn30E-0	208.5	0	0	0	113	0	2894	0	66	0
Mn30D-3	207.5	0	0	0	44	0	3077	0	68	0
Mn30D-2	206.4	0	0	0	45	0	3294	0	63	0
Mn30D-1	205	0	0	0	73	0	3256	0	74	0
Mn30C-3	202.7	0	0	0	51	0	3756	0	73	0
Mn30C	201	0	0	0	58	15	2826	0	72	0
Mn30C-2	199.9	0	0	0	44	0	3359	0	70	0
Mn30C-1	198.2	0	0	0	66	23	3159	0	82	0
Mn30B-6	197	0	0	0	77	28	3149	0	73	0
Mn30B-5	195.9	0	0	0	76	47	3130	0	75	0
Mn30B-4	195.1	0	0	0	82	41	3133	0	72	0
Mn29-8	191.5	0	0	39	291	151	2732	0	64	0
Mn30B	190.5	14	0	0	301	151	2611	0	52	0
Mn29-7	190.5	0	0	69	434	211	2610	0	74	0
Mn29U	190.3	0	0	38	315	179	2186	0	62	0
Mn29-6	189.7	7	0	31	851	486	1997	0	73	0
Mn29-5	189.2	57	0	59	559	378	1735	0	39	0
Mn29-4	188.3	43	44	76	342	306	2719	0	59	0
Mn29-2	187.1	48	0	0	1266	364	1964	0	47	0
Mn29L	186.7	6	0	42	155	265	1570	0	46	0
Mn29-1	186.5	22	0	33	1060	353	1703	0	50	0
Mn28-7	184	145	58	0	540	206	1660	0	38	0
Mn28-6	182.8	153	66	0	548	206	2100	0	41	0
Mn28-5	181.3	97	58	0	536	170	1905	0	51	0
Mn28	181	34	42	21	614	180	1524	0	44	0
Mn28-4	180.1	77	64	38	607	180	1816	0	49	0
Mn28-3	179.2	128	97	53	710	220	1102	0	34	0
Mn28-2	178.3	78	64	49	653	201	1815	0	38	30
Mn28-1	177.1	36	36	34	740	224	2163	0	51	25
Mn27	173	9	28	43	661	228	1396	0	59	46
Mn26	169	22	44	67	676	230	909	0	42	51
Mn25	161.5	21	14	22	737	185	2543	0	45	0

*Peak intensity of each mineral is normalized by the peak height of a standard quartz sample × 10000.
#Smectite peak height is corrected for chlorite contribution.

The amount of whitish, vesicular fragments decreases upward, and small amounts of angular, dark red, hematitic mudstone fragments are in the middle part. Granules are predominantly composed of flat and rounded fragments of light gray micritic limestone, gray cherty limestone, and grayish-black chert, probably derived from the underlying Pons Formation. Granules of angular, whitish, vesicular fragments are also present, especially in the basal part. The flat limestone and chert fragments show imbrication structure in places (Fig. 4A). Under the petrographic microscope, olive-green, flattened grains are replaced by chlorite and subordinate amount of granular pumpellyite, whereas the whitish vesicular fragments are grayish, dusty-looking, and composed of smectite with small amount of clinopyroxene microcrystals.

The upper part of unit 1 is characterized by flaser bedding (Fig. 4B) and wavy bedding (Fig. 4C). The ripple cross-laminated part consists of fine-grained, light greenish-gray, calcareous sandstone, which alternates with thin, grayish-black flaser and/or drapes of very fine grained, muddy sandstone. Under the petrographic microscope, the ripple cross-bedded sandstone is composed of recrystallized calcite grains, and small amounts of detrital plagioclase and quartz. The grayish-black muddy part is composed of clayey micritic matrix and opaque wisps of probable hematite, and small amounts of very fine grained detrital quartz and plagioclase, micritic limestone fragments, and foraminiferal skeletons. Although partly recrystallized, cross-laminations are still preserved. The estimated paleocurrent direction is consistently from S17° ± 10°E (Fig. 3).

TABLE 2. MAJOR ELEMENT COMPOSITION OF BULK SAMPLES DETERMINED BY X-RAY FLUORESCENCE ANALYSIS

Sample	Position (cm)	SiO_2 (wt%)	TiO_2 (wt%)	Al_2O_3 (wt%)	Fe_2O_3 (wt%)	MnO (wt%)	MgO (wt%)	CaO (wt%)	Na_2O (wt%)	K_2O (wt%)	P_2O_5 (wt%)	L.O.I. (wt%)	Total (wt%)
Mn32-2	227.1	5.37	0.05	1.37	0.60	0.06	0.45	49.70	n.d.	0.09	0.07	40.30	98.06
Mn32-1	225	6.55	0.07	1.81	0.71	0.06	0.51	48.71	n.d.	0.20	0.10	39.58	98.30
Mn32-0	223.3	5.47	0.07	1.53	0.64	0.06	0.47	49.70	n.d.	0.11	0.09	40.41	98.55
Mn31-5	221.6	6.01	0.08	1.75	0.76	0.07	0.53	48.32	n.d.	0.18	0.10	40.07	97.87
Mn31-4	219.8	6.84	0.08	1.86	0.77	0.07	0.52	49.32	n.d.	0.25	0.10	39.71	99.52
Mn31-3	218.4	7.18	0.08	2.02	0.85	0.07	0.56	49.20	n.d.	0.22	0.11	39.43	99.72
Mn31-1	215.5	5.41	0.06	1.51	0.65	0.06	0.49	48.79	n.d.	0.18	0.09	40.55	97.79
Mn30E-5	214.2	4.79	0.05	1.25	0.54	0.06	0.47	49.83	n.d.	0.10	0.08	40.81	97.98
Mn30E-4	213.1	5.24	0.06	1.38	0.59	0.06	0.52	50.56	n.d.	0.13	0.09	40.03	98.66
Mn30E-3	212	3.85	0.04	1.03	0.44	0.06	0.46	52.14	n.d.	0.04	0.07	41.43	99.56
Mn30E-2	210.9	3.39	0.04	0.97	0.43	0.05	0.51	52.32	n.d.	0.03	0.08	41.76	99.58
Mn30E-0	208.5	4.72	0.05	1.25	0.52	0.05	0.51	49.82	n.d.	0.08	0.08	41.00	98.08
Mn30D-2	206.4	2.60	0.03	0.83	0.36	0.05	0.46	51.95	n.d.	0.01	0.07	42.22	98.58
Mn30D-1	205	2.47	0.03	0.68	0.29	0.04	0.41	51.53	n.d.	0.03	0.06	42.29	97.83
Mn30C-3	202.7	2.15	0.02	0.62	0.24	0.05	0.38	51.93	n.d.	n.d.	0.05	42.49	97.93
Mn30C-2	199.9	2.28	0.03	0.65	0.26	0.05	0.43	53.14	n.d.	n.d.	0.06	42.47	99.37
Mn30B-4	195.1	4.95	0.06	1.32	0.58	0.05	0.47	48.83	n.d.	0.02	0.09	40.55	96.92
Mn30B-3	194	5.47	0.06	1.33	0.60	0.06	0.46	48.58	0.02	0.01	0.09	40.30	96.98
Mn30B-2	192.7	9.25	0.10	2.27	1.11	0.05	0.71	45.34	0.15	0.02	0.11	37.67	96.78
Mn29-9	191.9	9.46	0.11	2.46	1.21	0.05	0.84	45.97	0.28	0.01	0.12	37.34	97.85
Mn29-5	189.2	34.97	0.47	9.69	4.20	0.05	4.19	21.12	2.20	0.61	0.04	18.88	96.42
Mn29-4	188.3	29.28	0.66	8.87	4.21	0.05	4.34	24.90	1.33	1.22	0.04	22.23	97.13
Mn28-7	184	37.49	0.61	10.26	4.82	0.08	5.73	18.42	1.04	2.11	0.06	17.56	98.18
Mn28-6	182.8	39.84	0.58	11.07	4.97	0.05	6.30	17.20	1.01	2.34	0.06	16.51	99.93
Mn28-5	181.3	36.66	0.49	9.56	4.16	0.05	5.11	20.80	0.97	2.17	0.06	18.91	98.94
Mn28-4	180.1	39.77	0.55	10.56	4.62	0.07	5.93	17.54	1.06	2.42	0.06	16.41	98.99
Mn28-3	179.2	47.20	0.68	12.90	5.69	0.06	7.51	10.35	1.10	2.97	0.07	11.25	99.78
Mn28-2	178.3	42.39	0.57	10.94	4.81	0.06	6.29	15.94	1.14	2.39	0.07	15.11	99.71
Mn28-1	177.1	36.88	0.42	8.18	3.53	0.05	4.17	22.97	1.28	1.57	0.05	19.85	98.95
Mn27	173	43.52	0.57	10.70	4.71	0.05	6.68	16.07	1.88	2.03	0.07	14.25	100.53
Mn26	169	48.08	0.64	12.32	5.47	0.07	8.09	11.06	1.75	2.49	0.06	10.92	100.95
Mn25	161.5	35.41	0.33	6.50	2.74	0.06	4.28	27.04	1.27	1.09	0.06	22.64	101.42
Mn24	158.5	39.91	0.46	9.08	3.94	0.05	5.47	20.69	2.04	1.29	0.05	17.99	100.97
Mn23	152	31.13	0.33	7.37	2.72	0.07	3.06	30.05	2.35	0.47	0.07	24.20	101.82
Mn22.5	148.5	33.61	0.39	7.68	3.24	0.09	3.91	28.25	2.04	0.23	0.11	21.98	101.53
Mn22	144	32.38	0.37	7.37	3.04	0.08	3.26	29.87	1.96	0.31	0.10	23.15	101.89
Mn21	136	50.67	0.77	14.48	6.07	0.06	8.44	7.24	1.71	3.27	0.06	8.21	100.98
Mn20	129	51.26	0.90	15.57	6.86	0.06	8.38	5.01	1.48	3.96	0.05	6.58	100.11
Mn19	124.5	34.20	0.35	7.22	2.96	0.10	2.67	29.43	1.74	0.38	0.13	22.67	101.85
Mn18	120.5	41.21	0.47	9.40	3.91	0.08	3.68	23.27	2.23	0.37	0.13	17.17	101.92
Mn17	113	43.25	0.53	10.26	4.36	0.07	5.82	17.87	1.39	1.82	0.06	15.93	101.36
Mn16	111	49.23	0.56	11.36	4.95	0.05	6.38	12.52	1.42	2.02	0.05	12.22	100.76
Mn15	100	51.15	0.61	12.13	5.22	0.11	7.47	10.30	1.39	2.29	0.06	10.82	101.55
Mn14	94	46.80	0.59	11.59	4.90	0.12	6.28	14.26	1.67	1.83	0.05	13.50	101.59
Mn13	89	24.88	0.21	5.06	1.86	0.12	1.72	36.82	1.48	0.29	0.11	29.05	101.60
Mn12	85	20.22	0.20	4.41	1.76	0.12	2.00	39.94	1.10	0.11	0.13	31.86	101.85
Mn11	79	33.94	0.39	8.67	3.83	0.06	4.45	25.30	1.69	0.70	0.06	21.31	100.40
Mn10.5	75	21.80	0.18	4.53	1.78	0.13	2.28	38.96	0.98	0.24	0.12	30.63	101.63
Mn9	63	43.42	0.49	9.21	4.27	0.08	7.79	17.87	0.85	1.82	0.05	15.85	101.70
Mn8	58.5	45.73	0.46	8.64	3.86	0.08	6.59	18.55	0.98	1.45	0.04	15.55	101.93
Mn7	50	48.18	0.65	12.02	5.88	0.07	10.03	10.14	1.05	2.57	0.07	10.58	101.24
Mn5	35.5	48.58	0.67	12.36	5.63	0.06	9.79	9.82	0.98	2.40	0.05	10.72	101.06
Mn3	11	50.39	0.59	11.03	4.63	0.05	8.14	12.00	1.38	1.05	0.05	12.08	101.39
Mn2	5	48.18	0.60	11.14	4.75	0.06	9.04	11.78	1.46	1.01	0.04	12.61	100.67
Mn1	−3	2.61	0.01	0.48	0.15	0.07	0.60	53.50	0.07	n.d.	0.03	42.49	100.01

Units 2, 3, and 4 are composed of thin-bedded to parallel-laminated (0.5–2 cm thick), pale olive, medium- to fine-grained, calcareous sandstone with intercalations of millimeter-thick, pale greenish-yellow lamina (Fig. 4D) in the lower part, and wavy- to lenticular-bedded and ripple cross-laminated, light gray, finer grained, calcareous sandstone with grayish-black, very fine, sandy mudstone drapes in the upper part (Fig. 4E), although only parallel laminations are observed in unit 4. Under the petrographic microscope, the pale olive sandstone is predominantly composed of grayish, dusty, and occasionally vesicular fragments (corresponding to whitish vesicular fragments), pale yellowish-green, transparent stringers, highly deformed and flattened grains of probable chlorite, micritic limestone fragments, and subordinate amounts of detrital

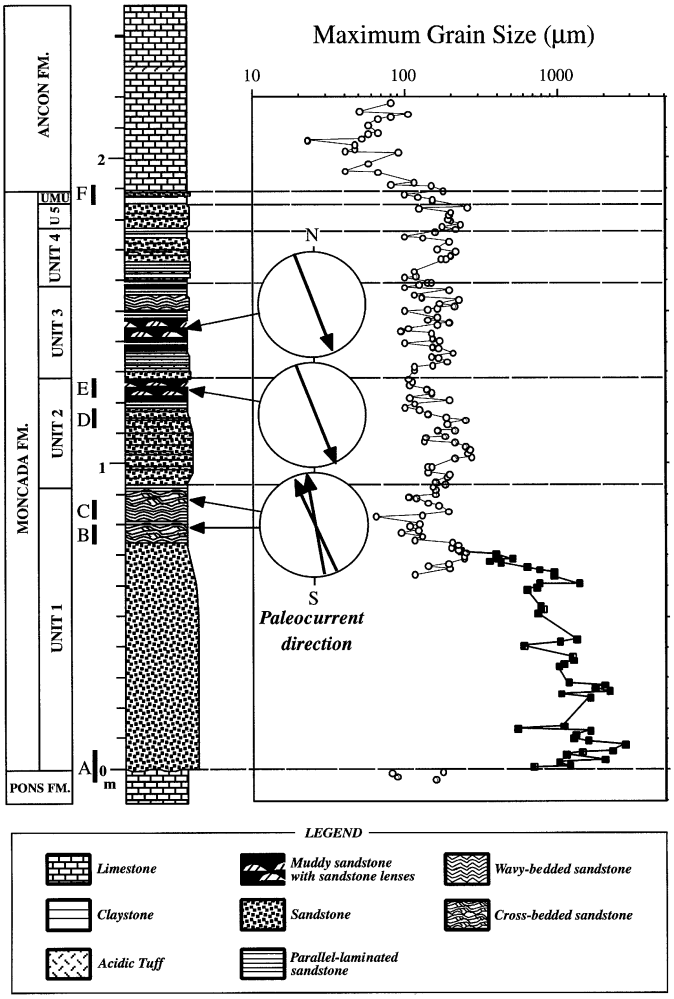

Figure 3. Columnar section of Moncada Formation. UMU means uppermost unit. Also shown on right side of column is maximum size of detrital silicate grains (open circle) and limestone and chert lithics (solid square), and paleocurrent directions measured at positions indicated by arrows. Positions of photographs A–F in Figure 4 are indicated on left side of column. Fm.—Formation.

quartz, chert, and plagioclase grains. The maximum detrital grain size varies within each thin bed; finer grain sizes are in its margins (Fig. 3). The composition of the light gray sandstone and grayish-black sandy mudstone in the upper part is basically the same as in unit 1, although foraminiferal skeletons become more common in these units. Light gray, wavy beds and lenses tend to be recrystallized; however, some of the ripple cross-laminations are still preserved. The estimated paleocurrent direction within two horizons in the upper part of units 2 and 3 is from N20° ± 15° W and N10° ± 15° W, respectively, which is approximately reversed from the directions observed in unit 1 (Fig. 3).

Unit 5 is composed of thin-bedded, light olive-brown, fine- to very fine grained, calcareous sandstone, separated by a millimeter-thick, pale greenish-yellow lamina. Under the petrographic microscope, the sandstone is composed of brownish-gray, dusty, vesicular fragments, micritic limestone and chert fragments, and other sedimentary lithics, including hematitic, silty, mudstone, and sandstone. No ripple cross-laminations or thin, parallel laminations are recognized in the upper part of this unit.

Calcareous claystone and very fine sandstone alternation (uppermost unit)

A 3–5-cm-thick unit of light colored, calcareous claystone and dark colored, very fine calcareous sandstone alternations (Fig. 4F) overlies the sandstone complex. A 1–4.5-cm-thick bed of light gray to dusty yellow, calcareous, sandy claystone containing thin, discontinuous lamina of light gray, calcareous, fine sandstone covers a slightly undulating surface of the underlying sandstone complex. This claystone is overlain by 1-cm-thick, olive-gray, fine sandstone, which is characterized by a yellowish rim at its upper and lower boundaries. The lower boundary of this sandstone bed is sharp, whereas the upper boundary is slightly bioturbated. Under the petrographic microscope, the light colored claystone consists of micritic calcite matrix with chert fragments and detrital quartz floating in its lower part, whereas the olive-gray sandstone consists of micritic limestone fragments, recrystallized calcite grains, brownish, dusty, vesicular fragments, and detrital quartz and plagioclase. The upper and lower margin of the bed, where the color is yellowish, is extensively cemented by pale yellowish-green, transparent chlorite.

Mineral and major element composition

The petrography of the Moncada Formation suggests the presence of systematic compositional variations within each unit, associated with variation in sedimentary structures and grain size. In order to characterize this compositional variation semiquantitatively, mineral and major element compositions were examined.

Calcite, quartz, plagioclase, and clay minerals, such as chlorite, illite, and smectite, are the major constituents of the Moncada Formation; pumpellyite and hematite are present in trace amounts. Within each unit, the calcite and plagioclase contents are lower in the lower part and gradually increase in the upper part, whereas those of quartz and clay minerals are higher in the lower part and gradually decrease in the upper part (Fig. 5). An exception is unit 4, where this trend is less clear. In the uppermost unit, dark colored, very fine calcareous sandstone is enriched in calcite, chlorite, and illite, whereas light colored calcareous claystone is enriched in quartz and plagioclase.

Major element compositions also show significant variation. SiO_2, TiO_2, Al_2O_3, Fe_2O_3, MgO, and K_2O are enriched in the lower part and decrease upward within each unit, whereas CaO, MnO, Na_2O, and P_2O_5 show the opposite trend (Fig. 5).

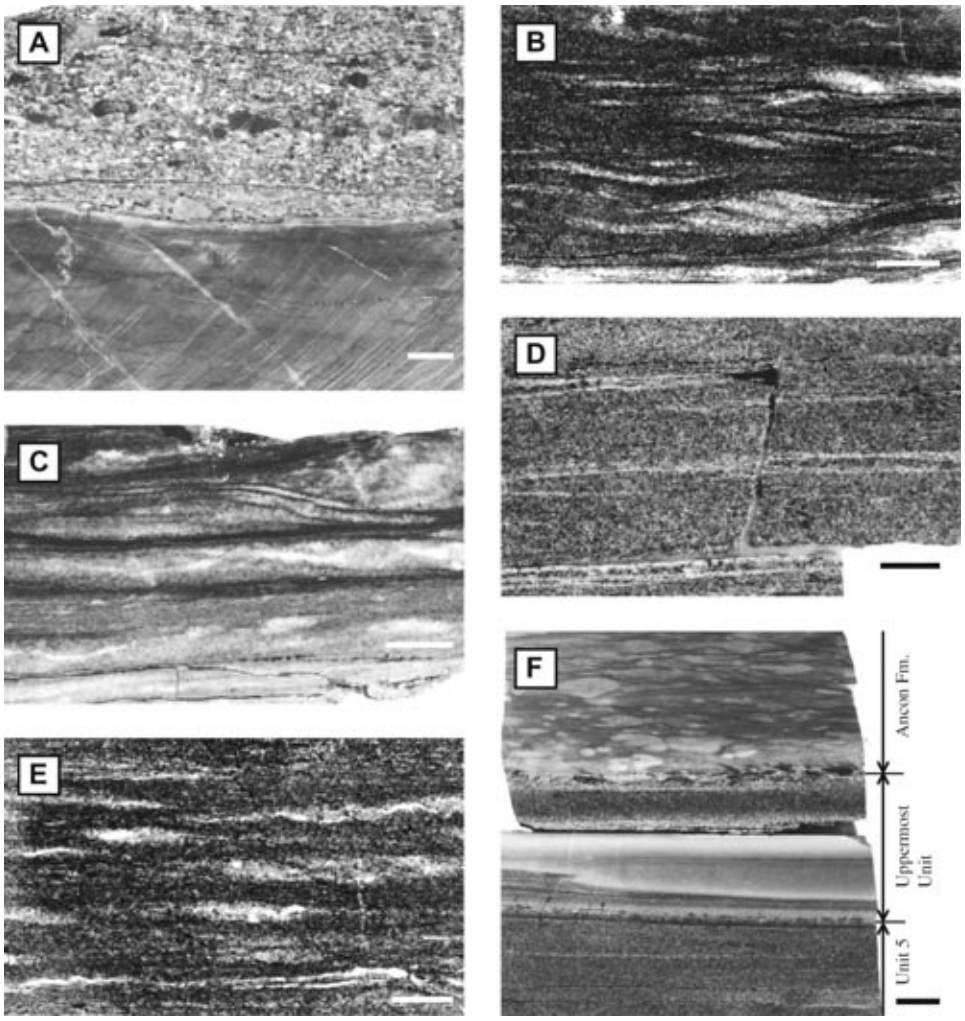

Figure 4. Photographs of typical lithology of Moncada Formation. Scale bar in lower right corner in each photograph is 1 cm. A: Slightly undulating erosional contact between grayish-black limestone of Pons Formation and calcareous sandstone of Moncada Formation. Flat granules in basal part of Moncada Formation show imbrication. B: Flaser bedding with ripple cross-laminations in upper part of unit 1 (Mn22-11). C: Wavy bedding with thin mud drape in upper part of unit 1 (Mn22-12). D: Thin beds of pale olive-gray medium to fine sandstone with thin, pale greenish-yellow lamina in unit 2 (Mn22-17). E: Lenticular beds with muddy sandstone drapes in upper part of unit 2 (Mn22-19). F: Uppermost unit of Moncada Formation. Light gray claystone with thin sandstone lamina in its lower part covers slightly undulating surface of sandstone complex, and it is covered by 1-cm-thick, olive-gray sandstone. Fm.—Formation.

These patterns reflect dilution effects by $CaCO_3$. However, even after normalization to Al_2O_3, a systematic compositional variation within each unit is still observable, especially for Fe_2O_3/Al_2O_3, MgO/Al_2O_3, K_2O/Al_2O_3, and TiO_2/Al_2O_3 ratios (Fig. 5).

The intervals with higher contents of quartz and clay minerals are less calcareous, and generally coincide with intervals with higher Fe_2O_3/Al_2O_3, MgO/Al_2O_3, K_2O/Al_2O_3, and TiO_2/Al_2O_3 ratios. These intervals also correspond to coarse-grained, olive-green to pale olive sandstone that is enriched in whitish, vesicular fragments and/or flattened, olive-green grains. According to petrographic observations in conjunction with energy-dispersive spectrometry (EDS) analysis, flattened, olive-green grains are replaced by chlorite, illite, and pumpellyite, whereas vesicular fragments are replaced by smectite. Considering the chemical composition of these grains, higher Fe_2O_3/Al_2O_3, MgO/Al_2O_3, and K_2O/Al_2O_3 ratios are attributable to the flattened, olive-green grains.

The intervals with higher contents of calcite and plagioclase generally coincide with intervals with higher CaO, MnO, Na_2O, and P_2O_5 contents, and correspond to medium- to fine-grained, light gray, calcareous sandstone, alternating with grayish-black, very fine grained, sandy mudstone. Higher concentrations of Na_2O are attributable to plagioclase, whereas higher concentrations of CaO and MnO are attributable to calcite.

There are also variations in the mineral and major element compositions between the units. Most conspicuous is the distribution of chlorite versus smectite: i.e., chlorite content is high in units 1 and 4 and nearly absent in units 2 and 3, whereas smectite and illite show the opposite trend. In unit 5, the chlorite content is high in the lower half, whereas smectite content is high in the upper half. Although less conspicuous, plagioclase shows a trend similar to that of smectite, with slightly higher concentrations in units 2 and 3. This trend is also observed in a slightly lower MgO/Al_2O_3 ratio in units 2 and 3 (Fig. 5).

BASAL PART OF THE ANCÓN FORMATION

The basal 0.5 m of the Ancón Formation consists of dark gray, flaggy limestone; the rest of the formation is characterized by light violet, slaty limestone. Dark gray, flaggy limestone of

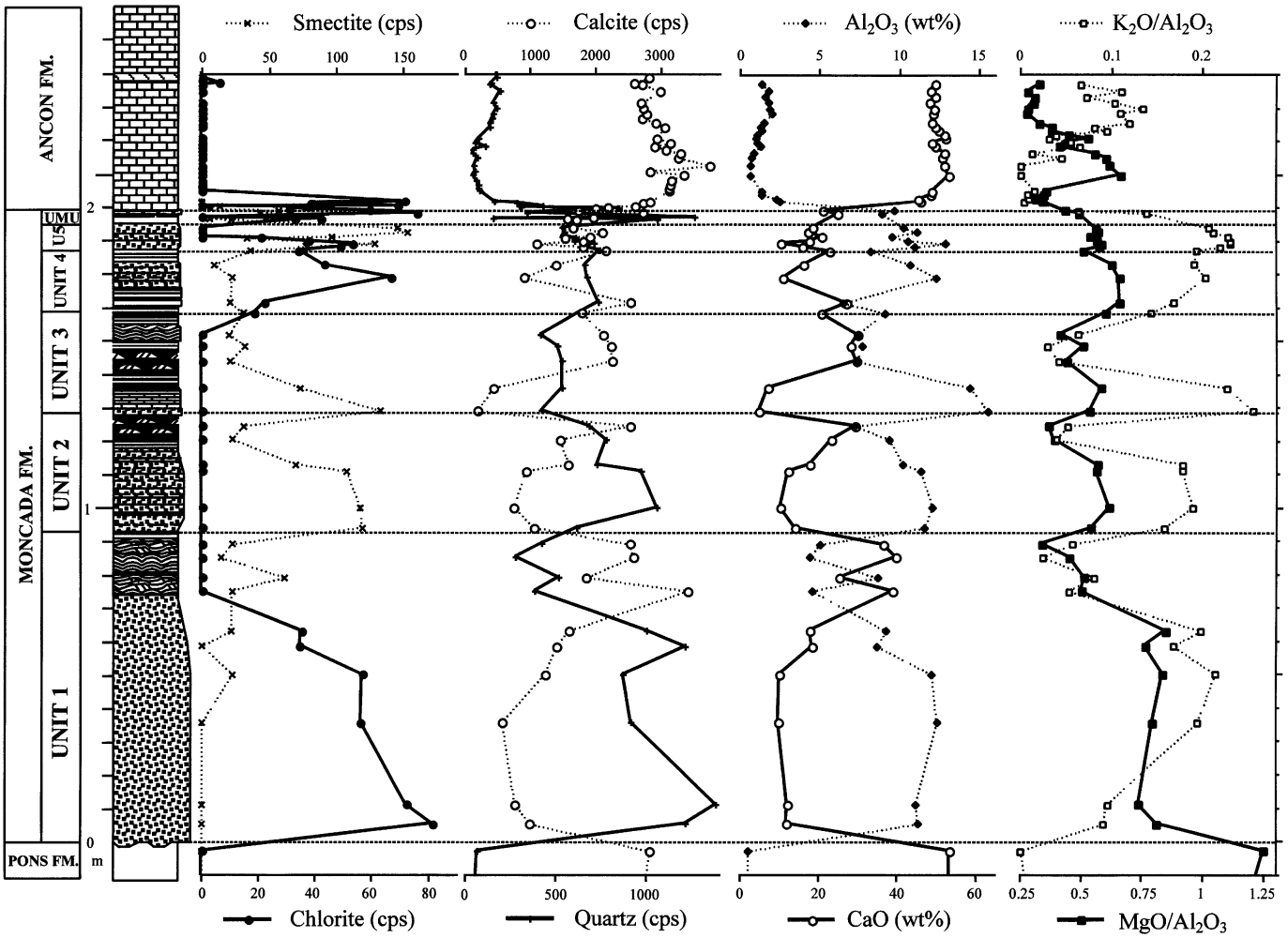

Figure 5. Diagrams showing vertical variations of mineral and chemical compositions in Moncada Formation. Legend for columnar section is same as in Figure 3. Peak intensity of each mineral is expressed as cps (count per second), which is normalized to condition that peak height of standard quartz sample is 10000 cps. Fm.—Formation.

the Ancón Formation conformably overlies the Moncada Formation with a gradational contact (Fig. 3). The basal 0.5 cm of the limestone is a strong dusty yellow that gradually fades out within next 8 cm interval. Flattened burrows of ~1 cm in diameter are abundant, especially in the basal 3 cm interval. Stylolites develop every 0.2–1.5 cm, which causes the flaggy appearance. Under the petrographic microscope, the flaggy limestone consists of a micritic matrix with a small amount of poorly preserved, small (30–60 μm in diameter), foraminiferal skeletons scattered in the matrix. Although we could not identify these foraminifera, their small size suggests earliest Danian age (P0 zone). Detrital grains, such as quartz and feldspar, are very rare and <50 μm.

PROBABLE RELATION OF THE MONCADA FORMATION WITH K-T BOUNDARY IMPACT

In order to explore the possible relation of the Moncada Formation with the K-T boundary impact, we determined the Ir concentrations in 26 samples (Table 3; Fig. 6). As is obvious from Figure 6, the Ir concentration in the grayish-black limestone of the underlying Pons Formation is ~10 ppt, which is within the range of ordinary crustal rocks (<100 ppt; after Koeberl, 1998). The Ir concentration in the lower to middle part of the sandstone complex is also low, below 50 ppt, whereas it increases to 138 ppt in the upper part of unit 5 where the sandstone color becomes slightly brownish. The Ir concentration further increases to 450 ppt in the 1-cm-thick light gray claystone, and decreases to 220 ppt in the 1-cm-thick olive-gray sandstone in the uppermost unit. A second Ir peak of 820 ppt occurs in the basal 1 cm of the Ancón Formation, where the color of the limestone is dusty yellow. The Ir concentration remains relatively high, between 335 and 396 ppt, to 13 cm above the base of the Ancón Formation, then decreases to 117 ppt within the next 3 cm interval. However, this level is still high compared to ordinary crustal rocks, especially taking into account the dilution effects of $CaCO_3$ in these rocks (Fig. 6).

TABLE 3. IR ABUNDANCE

Sample	Position (cm)	Concentration (ppt)
Mn32-2	227.05	13 ± 14
Mn31	213.00	32 ± 13
Mn30B-5	195.90	117 ± 14
Mn30B-4	195.05	191 ± 21
Mn30B-3	194.00	201 ± 11
Mn30B-2	192.70	335 ± 13
Mn29-9	191.90	376 ± 33
Mn29-8	191.45	396 ± 23
Mn29-7	190.50	663 ± 17
Mn29U	190.25	815 ± 31
Mn29-6	189.65	616 ± 17
Mn29-5	189.15	279 ± 14
Mn29M	188.30	217 ± 24
Mn29-4	188.30	160 ± 17
Mn29-3	187.50	194 ± 27
Mn29-2	187.10	380 ± 22
Mn29-L	186.70	448 ± 22
Mn29-1	186.45	390 ± 15
Mn28-7	183.95	138 ± 12
Mn28-6	182.75	88 ± 9
Mn28-5	181.30	122 ± 11
Mn28	181.00	46 ± 36
Mn28-2	178.30	75 ± 8
Mn8	58.50	50 ± 12
Mn2	5.00	21 ± 3
Mn1	−3.00	10 ± 4

The Ir peak position at the top of the sandstone complex and a peak Ir concentration of 820 ppt in the Moncada section is comparable to the Ir peak concentration reported from shallow-water K-T boundary sites in the Gulf of Mexico region (e.g., Smit et al., 1996).

We also searched for impact ejecta within the Moncada Formation. Quartz grains with planar deformation features (PDF) are commonly found throughout the formation (Fig. 7A). Our preliminary semiquantitative observation suggests that ~18% of detrital quartz grains have PDFs. The crystallographic orientations of PDFs in quartz from the Moncada Formation were measured using a universal stage with five axes (Montanari and Koeberl, 2000). As shown in Figure 8, the orientations strongly support their impact shock origin (e.g., Stöffler and Langenhorst, 1994). As for olive-green, flattened, and deformed grains, it is difficult to identify the original texture, which could be indicative of their origin. However, considering that they are replaced by chlorite and pumpellyite, the original material should have been an unstable material, such as impact glass enriched in Mg, Fe, and Ca.

Thin-section observation in conjunction with EDS analysis of angular, whitish, vesicular fragments suggests that they are composed of a mixture of smectite and small clinopyroxene crystals that show quench textures (Fig. 7B). Such quench textures of clinopyroxene are only found in microkrystites, impact melt rocks, and deep-sea basalt (Glass and Burns, 1988; Schuraytz et al., 1994; Smit, 1999; Bryan, 1972). Together with the highly vesicular nature and relatively large size of the grains, these whitish vesicular fragments are most likely of impact melt origin.

The presence of a significant peak in the Ir abundance in the uppermost unit of the Moncada Formation, as well as the presence of shocked quartz and vesicular glass fragments with pyroxene quench textures throughout the formation, strongly argues for a genetic relation of the Moncada Formation with meteorite impact. Together with its biostratigraphically estimated age of between late Maastrichtian and early Paleocene and its proximity to the Chicxulub crater, this evidence strongly suggests a K-T boundary impact origin for the Moncada Formation.

DEPOSITIONAL MECHANISM OF THE MONCADA FORMATION

Although it seems evident that the deposition of the Moncada Formation was associated with the K-T boundary impact, its genetic relation with the impact is not well understood. Detailed examination of sedimentary structures, as well as grain size and composition, should give some clues for the depositional mechanism.

The sandstone complex of the Moncada Formation is characterized by repetition of sandstone units with an overall upward decrease in grain size and unit thickness. Each unit shows systematic upward changes in sedimentary structure, from thin parallel beds, to parallel laminations, to flaser and/or lenticular bedding with ripple cross-laminations. These sedimentary structures suggest deposition from a flowing current. The maximum grain sizes for thin, parallel-bedded sandstone, parallel-laminated sandstone, and flaser-bedded sandstone are between ~0.2 and 0.3 mm, ~0.22 and 0.12 mm, and ~0.15 and 0.1 mm, respectively, suggesting that changes in these sedimentary structures reflect a gradual decrease in current speed. It is likely that thin, parallel beds to parallel laminations represent flat beds in an upper flow regime, whereas ripple cross-laminations represent ripples in a lower flow regime (e.g., Friedman and Sanders, 1978). Thus, the systematic changes in sedimentary structures and an upward decrease in grain size, especially in units 1 and 2, most likely reflect an upward decrease in flow speed within the units. The pattern of the maximum grain-size variation within a unit becomes more symmetrical in units 3, 4, and 5. Several centimeter-scale oscillations in the maximum grain size are observable within each unit, probably reflecting shorter scale oscillations in current speed.

The paleocurrent direction estimated from ripple cross-laminations is unidirectional within individual units, whereas reversing paleocurrent direction is observed between units 1 and 2. The direction is unchanged between units 2 and 3. The paleocurrent direction is from S17° ± 10°E in unit 1 and from N15° ± 20°W in units 2 and 3. These paleocurrent directions should be corrected for crustal rotation, and our preliminary paleomagnetic measurement of the Moncada Formation (three samples) indicates counterclockwise rotation of ~22°. After

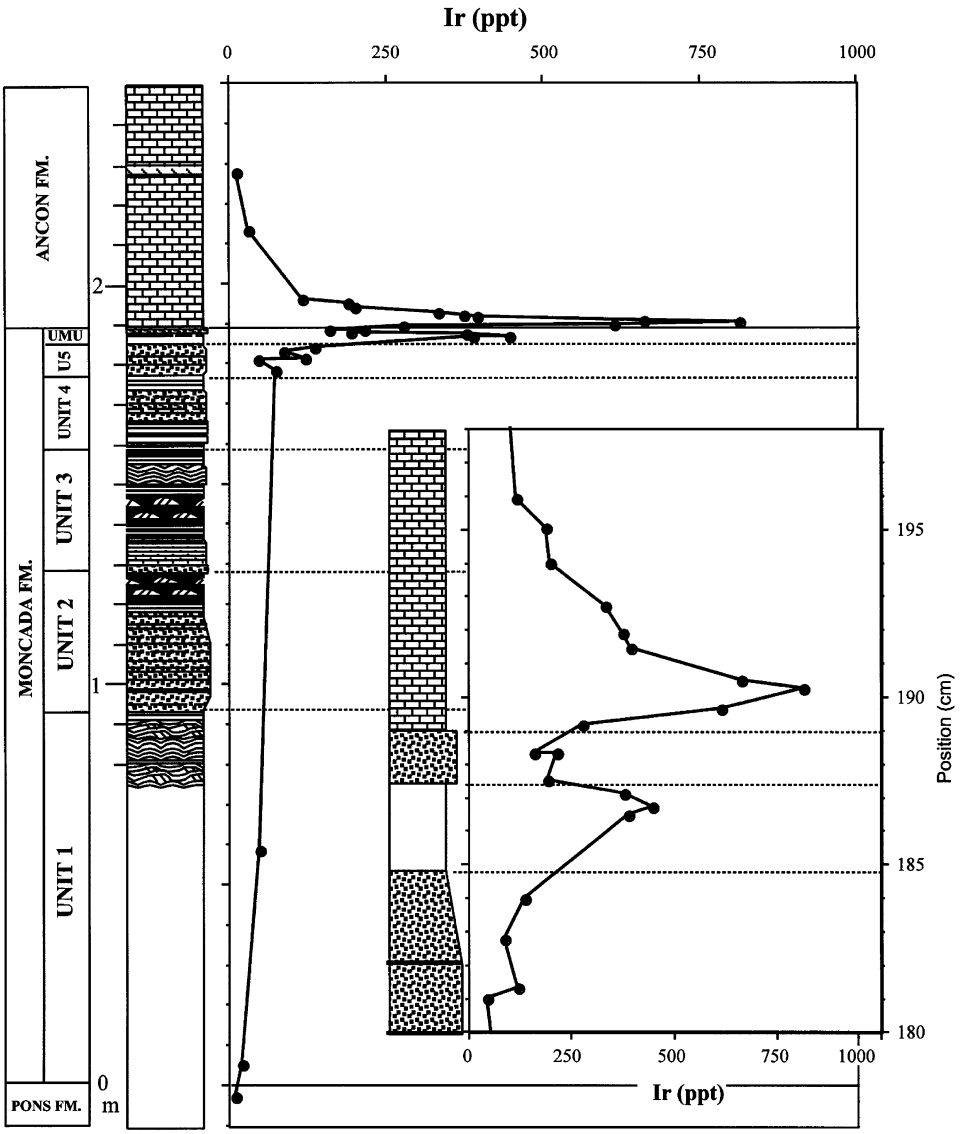

Figure 6. Variation of Ir concentration across Moncada Formation. Magnification of 180–198 cm interval, covering uppermost unit (UMU), is inserted in right lower corner. Legend for columnar section is same as in Figure 3. Fm.—Formation.

correcting for the crustal rotation, the current direction for the Moncada Formation is S5°W and N7°E, nearly parallel to the eastern margin of the Yucatan platform.

The mineral and major element compositions within each unit also vary systematically (Fig. 5), probably reflecting an upward decrease in current speed. Variations in mineral and chemical compositions, in conjunction with petrographic observation, suggest that coarse grains are dominated by ejecta materials, such as altered, vesicular, impact-melt fragments and shocked quartz grains, and flattened olive-green grains of possible altered impact glass, whereas material reworked from underlying substrates, such as calcareous microfossils, detrital plagioclase, and sedimentary lithic fragments, is predominantly fine grained. Further examination revealed that mineral and chemical compositions in the lower (and coarser) part of individual units, especially the relative abundance of smectite and illite versus chlorite, are different between units 1, 4, and 5, and units 2 and 3. This may reflect changes in provenance in response to the changes in paleocurrent direction; unit 1, which is characterized by high chlorite content, has an opposite current direction compared to units 2 and 3, which are characterized by high smectite and illite contents. Assuming that chlorite and smectite represent flattened, olive-green grains of possible altered impact glass and altered, vesicular, impact-melt fragments, respectively, possible altered impact glass and altered, vesicular, impact-melt fragments might have been derived from southern and northern directions, respectively. If this interpretation is correct, units 4 and 5 were also derived from the north.

It is difficult to estimate the bathymetry of the Moncada Formation at the time of impact, because of the lack of late Maastrichtian strata underneath the Moncada Formation, and poor preservation of depth-diagnostic microfossils in the over-

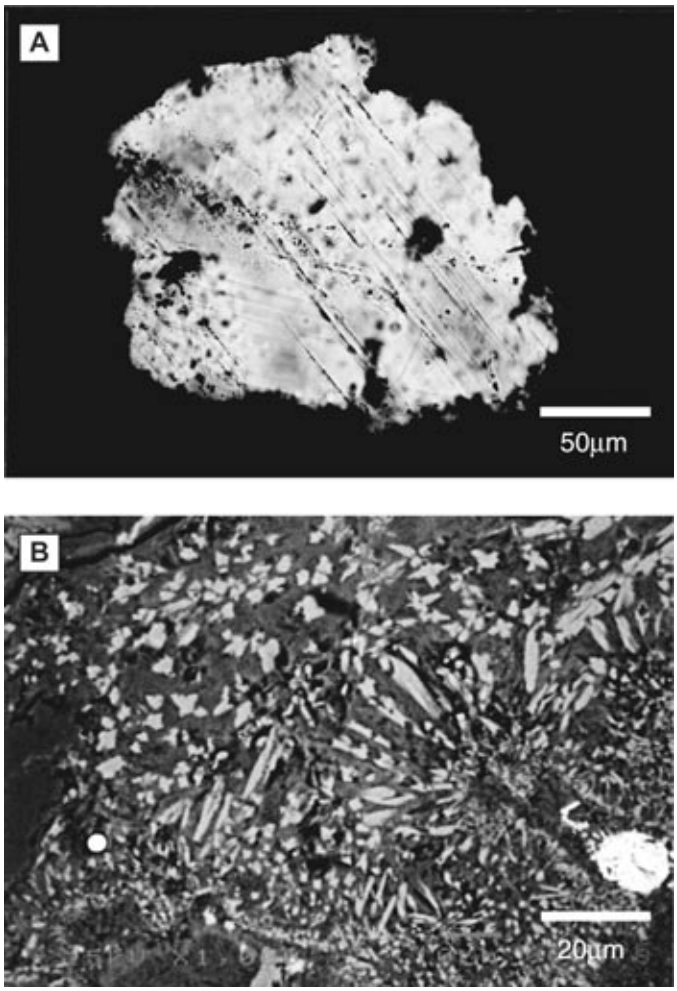

Figure 7. Thin-section photographs of ejecta materials in Moncada Formation. A: Detrital quartz grain (240 μm) with two sets of planar deformation features (PDF) from unit 5 (Mn22-28). Each set of PDFs is parallel to ω(23°). Cross-polarized light. B: Whitish, vesicular fragments with clinopyroxene quench textures. Light gray, blade-like, fine crystals are clinopyroxene. Gray matrix is smectite, which is probably altered from impact glass. Spherical aggregate of bright needle-like grains on right side is composed of goethite, dark gray grain on left side is quartz, and gray grain on lower left is chlorite. Back-scattered electron image.

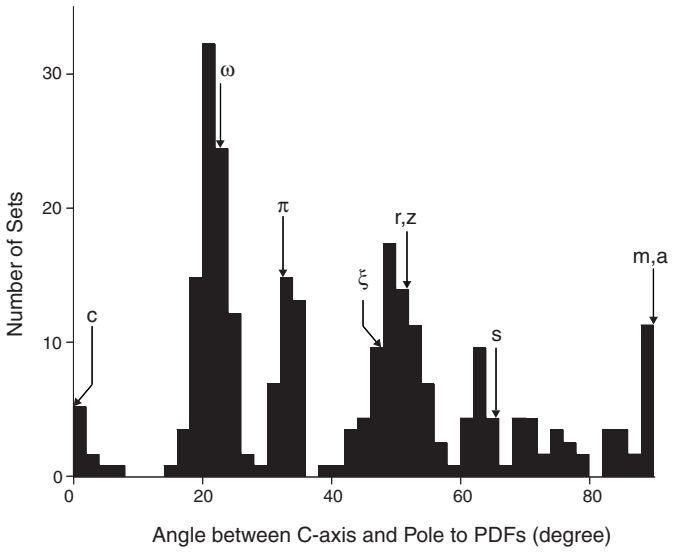

Figure 8. Histogram showing variation in angle between c-axis and pole to planar deformation features (PDF) in shocked quartz grains obtained from Moncada Formation. Crystallographic orientations of c(0°), ω(22.95°), π(32.42°), ξ(47.73°), r, z(51.79°), s(65.56°) and m, a(90°) are prominent, indicating their impact-derived origin (Stöffler and Langenhorst, 1994). We measured 303 sets in 187 grains. Samples were selected from 58–64 cm (unit 1), 77–85 cm (unit 1), 113–120 cm (unit 2), 152–158 cm (unit 3), 168–171 cm (unit 4), and 180–185 cm (unit 5).

lying Ancón Formation. However, the lower part of the Ancón Formation is very fine grained, calcareous, and free of turbidites, suggesting a hemipelagic to pelagic environment of deposition. Considering that the calcium carbonate compensation depth in the Atlantic during the early Paleocene has been <3.3 km (van Andel, 1975), and that the Ancón Formation is highly calcareous, the depositional depth of the Moncada Formation should have been shallower than 3.3 km. The paleotectonic reconstruction suggests that the Los Organos belt was located immediately to the east of the eastern margin of the present Yucatan block and was scraped off this margin in the course of northward movement of the Cretaceous volcanic arc during the late Paleocene to early Eocene (Iturralde-Vinent, 1994, 1998). According to Rosencrantz (1990), the eastern margin of Yucatan (the Yucatan borderland) is an offshore continuation of the Yucatan platform, and Paleogene-Late Cretaceous deep-water clastics were found in offshore wells to the east of Belize. Although the bathymetry of these deep-water clastics is not clear, they most likely represent a slope facies. Because the Los Organos belt is considered to have been located immediately to the east of the Yucatan borderland, the Moncada Formation should have been deposited in a slope setting with a probable paleodepth between 0.2 and 3.3 km.

The depositional mechanism for each unit should explain the unidirectional flow with a gradual upward decrease in flow speed. The mechanism should also explain the paleocurrent direction subparallel to the Yucatan platform margin, as well as paleocurrent reversal between the units. Turbidity currents are one possibility. Longitudinal paleocurrent direction with paleocurrent reversal between different units could be explained by turbidites filling a trench-type basin plain (e.g., Hesse, 1974). However, a gradational contact at the base of each unit (except unit 1), the symmetric maximum grain-size-variation patterns, especially in units 4 and 5, the presence of centimeter-scale oscillations of maximum grain size within each unit, and the lack of hemipelagic claystone at the top of each unit, taken together, are inconsistent with a turbidite origin for individual units. Moreover, a trench-type basin-plain setting required to explain longitudinal paleocurrent direction with reversals is inconsistent with the continental slope setting as estimated here, and a systematic upward decrease in unit thickness without any

interruptions by hemipelagic deposition are difficult to explain by a turbidite origin. Explanation that the entire sandstone complex represents a single turbidite bed is also inconsistent with paleocurrent reversals within the sandstone complex.

K-T boundary sandstone complexes as thick as 9 m deposited on shelf to upper slope environments are reported from multiple sites in the Gulf of Mexico region, and they are interpreted as being formed as a result of tsunamis generated by the K-T boundary impact (Bourgeois et al., 1988; Smit et al., 1996; Smit, 1999). The sandstone complexes in Mexico (Smit et al., 1996; Smit, 1999) are especially similar to the sandstone complex of the Moncada Formation with respect to such characteristics as (1) repetition of upward-fining units, (2) reversing current directions between the units, (3) systematic upward decreases in unit thickness, and (4) the high concentration of Ir at the top of the sandstone complex. In addition, the number of units in the Moncada sandstone complex is comparable to those in the Gulf of Mexico region (as many as seen, according to Smit et al., 1996). The first three characteristics strongly support a tsunami origin for the sandstone complex of the Moncada Formation, as was proposed for the K-T sandstone complexes in Mexico (Smit et al., 1996).

Major differences between the sandstone complex of the Moncada Formation and those of Mexico are the patterns of paleocurrent reversals and the paleocurrent directions with respect to the paleoshoreline. Smit et al (1996) described paleocurrent reversals between every subsequent unit of the K-T sandstone complex in La Lajilla, Mexico, whereas paleocurrent direction is reversed every two units in the Moncada Formation. Although paleocurrent direction is not estimated directly for units 4 and 5, paleocurrent reversals are estimated between units 3 and 4, according to changes in the clay mineral assemblage and the MgO/Al_2O_3 ratio. Smaller scale oscillations in the maximum grain size observed within each unit suggest the presence of two to six higher frequency waves superimposed on larger amplitude, lower frequency waves. Thus, the pattern of current direction changes in the Moncada Formation is more complex than in Mexico. Such a complex tsunami wave rhythm could have been created by local reflection of tsunami waves due to the complex paleogeography of the region. Alternatively, multiple gravity flows triggered by seismic shocks of the impact (e.g., Takayama et al., 2000) might have caused multiple tsunami waves with a complex rhythm. The north-south-trending paleocurrent directions subparallel to the eastern margin of the Yucatan platform can be explained by the relatively deep depth of the studied site that prevented the wave direction from becoming parallel to the shoreline direction.

COMPARISON WITH OTHER K-T BOUNDARY DEPOSITS IN WESTERN CUBA

K-T boundary deposits at other sites in western Cuba are characterized by extremely thick (to 700 m) deposits, including a lower coarse-grained debris-flow unit and an upper calcarenite to calcilutite unit that shows normal grading (e.g., Takayama et al., 2000). The Moncada Formation, however, is only 2 m thick. The continental slope depositional setting of the Moncada Formation and its proximity to the southern gateway between the Yucatan platform and the Cretaceous volcanic arc may explain such a large difference in thickness. The absence of a basal debris-flow unit in the Moncada Formation, and the lack of a Turonian to Maastrichtian sedimentary sequence underneath it, suggests that the Turonian to Maastrichtian sequence was eroded by the debris flow before deposition of the Moncada Formation. Kiyokawa et al. (2000) demonstrated that the lower part of the Cacarajicara Formation is composed of an ~300-m-thick gravity-flow unit that is characterized by breccias of limestone and chert similar in appearance and age to those of the Upper Cretaceous sedimentary sequence in the Guaniguanico terrane. Iturralde-Vinent et al. (2000) estimated that the Cacarajicara Formation in the Rosario belt of the Guaniguanico terrane was deposited in the lower slope to basinal environment on the eastern frank of the Yucatan platform. Thus, it is likely that Moncada was located on the slope between the Yucatan platform to the west and the Rosario belt to the east, and was actually part of the source area for the debris-flow unit of the Cacarajicara Formation. On the basis of this interpretation, we consider that the debris flow triggered by the K-T boundary impact removed the Upper Cretaceous sedimentary sequence from the middle to upper slope of the eastern Yucatan margin, including Moncada, transported the sediment downslope, and deposited the thick K-T boundary deposits such as the Cacarajicara Formation in the deeper part of the proto-Caribbean basin. Consequently, no deposit corresponding to the debris-flow unit of the Cacarajicara Formation accumulated in Moncada.

The upper unit of K-T boundary deposits at other sites in western Cuba is composed of as much as 400 m of normally graded calcarenite to calcilutite, which Takayama et al. (2000) interpreted as a homogenite (a deep-sea tsunami deposit). The calcarenite part is 100–300 m thick at these localities, whereas the calcareous sandstone at the Moncada section is only 2 m thick. Our on-going high-resolution study of homogenite in the Peñalver Formation near Havana revealed slight but consistent oscillations in grain size and composition within the calcarenite part that repeated five to six times. This oscillation may suggest repeated agitation of the upper water column by tsunami waves, or lateral injection of the coarser material to the water column by backwash. For this reason, we consider that the calcarenite part of the homogenite was deposited at about the same time as the sandstone complex in Moncada. The difference in their thicknesses can be explained by the difference in their depositional depths. Assuming that the suspended sediment cloud created by tsunami agitation was widespread in the deeper part of the sea, its thickness should have increased with increasing water depth. Thus, thick calcarenite was deposited by vertical settling in the basinal sites, whereas the thin calcareous sandstone complex was deposited under the influence of tsunami waves in shallow sites.

The calcilutite part of these homogenite beds is 30–100 m

thick (Takayama et al., 2000; Kiyokawa et al., 2000), and is interpreted as being deposited from a low-concentration sediment suspension cloud within several days to weeks after the impact. However, calcareous claystone at the top of the Moncada Formation is only a few centimeters thick. This difference needs to be explained, especially if the sediment cloud prevailed throughout the water column within the proto-Caribbean basin. The proximity of the studied site to the southern gateway, in addition to its shallow bathymetry compared to other K-T boundary sites in western Cuba, could be one explanation. The surface current (western boundary current) flowing through the gateway between the Yucatan platform and the Cuban volcanic arc and continuing along the eastern margin of the Yucatan platform could have cleaned the upper ~500 m of the water column, especially in the southern part of the proto-Caribbean basin, and thus prevented deposition of thick calcilutite at the study site. Alternatively, it is possible that the sediment suspension cloud was restricted to the deeper part of the proto-Caribbean basin.

CONCLUSIONS

The Moncada Formation in western Cuba is a K-T boundary sandstone complex that is characterized by (1) abundant ejecta materials such as shocked quartz and altered impact-melt fragments throughout the formation, (2) the presence of an Ir-rich claystone at the top of the complex, (3) repetition of fining-upward sandstone units with a gradual upward decrease in thickness, (4) the occurrence of current ripples showing reversing paleocurrent direction between the units, and (5) the lack of hemipelagic clays between the units. These characteristics are similar to other K-T sandstone complexes in Mexico that are interpreted to have been formed by tsunamis caused by the impact. On the basis of these characteristics in conjunction with its biostratigraphically estimated age, between late Maastrichtian and early Paleocene, it is concluded that the Moncada sandstone complex was formed by repeated tsunami waves caused by the K-T impact.

Although similarities between the K-T sandstone complex of Moncada and those in Mexico are obvious, there are several differences. First, the inferred tsunami waves are not simple oscillatory waves, but had more complex rhythms, the first wave moving from south to north, and the subsequent two waves from north to south. Second, shorter scale grain-size oscillations within each unit are recognized, suggesting higher frequency waves superimposed on the lower frequency waves. Third, the depositional site was not on the shelf but on the slope; thus, the bathymetry was probably deeper than most of the other K-T boundary sandstone complexes in the Gulf of Mexico region. The lack of thick gravity-flow and homogenite-type deposits at Moncada probably reflects its slope setting, where the Turonian to Maastrichtian limestone and chert sequence was eroded, most likely by gravity flows triggered by the seismic shocks of the impact, and its proximity to the southern gateway that allowed influx of clear surface water. Better estimates of the bathymetry are needed to allow a more precise estimation of the magnitude and mode of the tsunami waves caused by the K-T boundary impact.

ACKNOWLEDGMENTS

We thank the Agencia Medio Ambiente in Cuba for their support of the field survey in Cuba. This research was made possible thanks to an agreement between the Department of Earth and Planetary Sciences, University of Tokyo, the Museo Nacional de Historia Natural (Agencia del Medio Ambiente) de Cuba, and the Instituto de Geologia del Ministerio del Industria Basica. We acknowledge especially the support provided to the field research in Cuba by Mitsui & Co., Ltd., as well as their manager in Havana, A. Nakata. We also thank C. Koeberl, B. Bohor, and P. Claeys, who critically read the manuscript and gave us many valuable suggestions, and J. Compton, who helped improve our English. The neutron activation analysis was carried out at the Inter-University Laboratory for the joint use of (Japan Atomic Energy Research Institute) Facilities. The survey was supported by grants-in-aid for scientific research of the Japan Society for the Promotion of Science (no. 11691116) and also by research funds donated to the University of Tokyo by NEC Corporation, I. Ohkawa, M. Iizuka., and K. Ihara.

REFERENCES CITED

Bohor, B.F., 1996, A sediment gravity-flow hypothesis for siliciclastic units at the K/T boundary, northeastern Mexico, *in* Ryder, G., Fastovsky, D., and Gartner, S., eds., The Cretaceous–Tertiary event and other catastrophes in Earth history: Geological Society of America Special Paper 307, p. 183–195.

Bourgeois, J., Hansen, T.A., Wiberg, P.L., and Kaufmann, E.G., 1988, A tsunami deposit at the Cretaceous–Tertiary boundary in Texas: Science, v. 241, p. 567–570.

Bralower, T.J., and Iturralde-Vinent, M.A., 1997, Micropaleontological dating of the collision between the North American plate and the Greater Antilles Arc in western Cuba: Palaios, v. 12, p. 133–150.

Bryan, W.B., 1972, Morphology of quench crystals in submarine basalts: Journal of Geophysical Research, v. 29, p. 5812–5819.

D'Hondt, S., Pilson, M.E., Sigurdsson, H., Hanson, A.F., Jr., and Carey, S., 1994, Surface-water acidification and extinction at the Cretaceous–Tertiary boundary: Geology, v. 22, p. 983–986.

Diaz Otero, C., Iturralde-Vinent, M.A., Garcia Delgado, D., 2000, The Cretaceous–Tertiary Boundary "Cocktail" in Western Cuba, Greater Antilles [abs.], in Catastrophic events and mass extinctions: Impact and beyond: Houston, Texas, Lunar and Planetary Institute, LPI Contribution No. 1053, p. 37–38.

Friedman, G.M., and Sanders, J.E., 1978, Principles of sedimentology: New York, John Wiley and Sons, 792 p.

Glass, B.P., and Burns, C.A., 1988, Microkrystites: A new term for impact-produced glassy spherules containing primary crystallites [abs.]: Lunar and Planetary Science Conference, 18th, Houston, Texas, Lunar and Planetary Institute, p. 455–458.

Hesse, R., 1974, Long-distance continuity of turbidites: Possible evidence for an Early Cretaceous trench-abyssal plain in the East Alps: Geological Society of America Bulletin, v. 85, p. 859–870.

Hildebrand, A.R., Penfield, G.T., Kring, D.A., Pilkington, M., Camargo, Z.A., Jacobsen, S.B., and Boynton, W.V., 1991, Chicxulub crater: A possible Cretaceous/Tertiary boundary impact crater on the Yucatán Peninsula, Mexico: Geology, v. 19, p. 867–871.

Irino T., and Tada, R., 2000, Quantification of aeolian dust (Kosa) contribution to the Japan Sea sediments and its variation during the last 200 ky: Geochemical Journal, v. 34, p. 59–93.

Iturralde-Vinent, M.A., 1992, A short note on the Cuban late Maastrichtian megaturbidite (an impact-derived deposit?): Earth and Planetary Science Letters, v. 109, p. 225–228.

Iturralde-Vinent, M.A., 1994, Cuban geology: A new plate-tectonic synthesis: Journal of Petroleum Geology, v. 17, p. 39–70.

Iturralde-Vinent, M.A., 1995, Sedimentary geology of Western Cuba, in SEPM Congress on Sedimentary Geology, 1st Field Trip Guidebook: St. Petersburg, Florida, (SEPM) Society for Sedimentary Geology, 21 p.

Iturralde-Vinent, M., 1998, Sinopsis de la constitución geológica de Cuba, *in* Melgarejo, J.C., and Proenza, J.A., eds., Geología y metalogenia de Cuba: Una introducción: Acta Geológica Hispanica, v. 33, nos. 1–4, p. 9–56.

Iturralde-Vinent, M.A., Garcia, D., Diaz, C., Rojas, R., Tada, R., Takayama, H., and Kiyokawa, S., 2000, The K/T boundary impact layer in Cuba: Update of an international project [abs.], in Catastrophic events and mass extinctions: Impact and beyond: Houston, Texas, Lunar and Planetary Institute, LPI Contribution No. 1053, p. 76–77.

Kiyokawa, S., Tada, R., Oji, T., Tajika, E., Nakano, Y., Goto, K., Yamamoto, S., Takayama, H., Toyoda, K., Rojas, R., Garcia, D., Iturralde-Vinent, M.A., and Matsui, T., 2000, More than 500 m thick K/T boundary sequence; Cacarajicara Formation, western Cuba [abs.], *in* Catastrophic events and mass extinctions: Impact and beyond: Houston, Texas, Lunar and Planetary Institute, LPI Contribution No. 1053, p. 100–101.

Koeberl, C., 1998, Identification of meteoritical components in impactites, *in* Grady, M.M., Hutchison, R., McCall, G.J.H., and Rothery, D.A., eds., Meteorites: Flux with time and impact effects: Geological Society [London] Special Publication 140, p. 133–152.

Kyte, F.T., Zhou, L., and Lowe, D.R., 1992, Noble metal abundances in an Early Archean impact deposit: Geochimica et Cosmochimica Acta, v. 56, p. 1365–1372.

Montanari, A., and Koeberl, C., 2000, Impact stratigraphy: The Italian record, *in* Bhattacharji, S., Friedman, G.M., Neugebauer H.J., and Seilacher, A., eds., Lecture Notes in Earth Sciences, Volume 93: Berlin, Springer-Verlag, p. 295–300.

Moore, D.M., and Reynolds, R.C., Jr., 1997, X-ray diffraction and the identification and analysis of clay minerals: Oxford, Oxford University Press, 378 p.

Potts, P.J., Tindle, A.G., and Webb, P.C., 1992, Geochemical reference material compositions: Rocks, minerals, sediments, soils, carbonates, refractories and ores used in research and industry: Caithness/Boca Raton, Lousiana, Whittles Publishing/CRC Press Inc., 313 p.

Pszczolkowski, A., 1986, Megacapas del maestrichtiano en Cuba occidental y central: Bulletin of the Polish Academy of Earth Science, v. 34, p. 81–94.

Rosencrantz, E., 1990, Structure and tectonics of the Yucatán basin, Caribbean Sea, as determined from seismic reflection studies: Tectonics, v. 9, p. 1037–1059.

Ryder, G., Fastovsky, D., and Gartner, S., editors, 1996, The Cretaceous–Tertiary event and other catastrophes in Earth history: Geological Society of America Special Paper 307, 569 p.

Schuraytz, B.C., Sharpton, V.L., and Marin, L.E., 1994, Petrology of impact-melt rocks at the Chicxulub multiring basin, Yucatán, Mexico: Geology, v. 22, p. 868–872.

Sigurdsson, H., D'Hondt, S., Arthur, M.A., Bralower, T.J., Zachos, J.C., van Fossen, M., and Channell, J.E.T., 1991, Glass from the Cretaceous/Tertiary boundary in Haiti: Nature, v. 349, p. 482–487.

Smit, J., 1999, The global stratigraphy of the Cretaceous–Tertiary boundary impact ejecta: Annual Reviews of Earth and Planetary Science, v. 27, p. 75–113.

Smit, J., Montanari, A., Swinburne, N.H.M., Alvarez, W., Hildebrand, A.R., Margolis, S.V., Claeys, P., Lowrie, W., and Asaro, F., 1992, Tektite-bearing, deep-water clastic unit at the Cretaceous–Tertiary boundary in northeastern Mexico: Geology, v. 20, p. 99–103.

Smit, J., Roep, Th.B., Alvarez, W., Claeys, P., Grajales-Nishimura, J.M., and Bermudez, J., 1996, Coarse-grained, clastic sandstone complex at the K/T boundary around the Gulf of Mexico: Deposition by tsunami waves induced by the Chicxulub impact?, *in* Ryder, G., Fastovsky, D., and Gartner, S., eds., Cretaceous–Tertiary event and other catastrophes in Earth history: Geological Society of America Special Paper 307, p. 151–182.

Stöffler, D. and Langenhorst, F., 1994, Shock metamorphism of quartz in nature and experiment. 1. Basic observation and theory: Meteoritics, v. 29, p. 155–181.

Takayama, H., Tada, R., Matsui, T., Iturralde-Vinent, M.A., Oji, T., Tajika, E., Kiyokawa, S., Garcia, D., Okada, H., Hasegawa, T., and Toyoda, K., 2000, Origin of the Peñalver Formation in northwestern Cuba and its relation to K/T boundary impact event: Sedimentary Geology, v. 135, p. 295–320.

Van Andel, T.J., 1975, Mesozoic/Cenozoic calcite compensation depth and the global distribution of calcareous sediments: Earth and Planetary Science Letters, v. 26, p. 187–194.

MANUSCRIPT ACCEPTED BY THE SOCIETY MARCH 22, 2001